Stable water isotope tracing through hydrological models for disentangling runoff generation processes at the hillslope scale

David Windhorst[1], Philipp Kraft[1], Edison Timbe[1,2], Hans-Georg Frede[1], Lutz Breuer[1]

[1] {Institute for Landscape Ecology and Resources Management (ILR), Research Centre for BioSystems, Land Use and Nutrition (IFZ), Justus-Liebig-Universität Gießen, Germany}

[2] {Departamento de Recursos Hídricos y Ciencias Ambientales, Universidad de Cuenca, Cuenca, Ecuador}

Correspondence to: D. Windhorst (david.windhorst@umwelt.uni-giessen.de)

12 **Abstract**

13 Hillslopes are the dominant landscape components where incoming precipitation is
14 transferred to become groundwater, streamflow or atmospheric water vapor. However,
15 directly observing flux partitioning in the soil is almost impossible. Hydrological hillslope
16 models are therefore being used to investigate the processes involved. Here we report on a
17 modeling experiment using the Catchment Modeling Framework (CMF) where measured
18 stable water isotopes in vertical soil profiles along a tropical mountainous grassland hillslope
19 transect are traced through the model to resolve potential mixing processes. CMF simulates
20 advective transport of stable water isotopes ^{18}O and ^{2}H based on the Richards equation within
21 a fully distributed 2-D representation of the hillslope. The model successfully replicates the
22 observed temporal pattern of soil water isotope profiles (R^2 0.84 and NSE 0.42). Predicted
23 flows are in good agreement with previous studies. We highlight the importance of
24 groundwater recharge and shallow lateral subsurface flow, accounting for 50% and 16% of
25 the total flow leaving the system, respectively. Surface runoff is negligible despite the steep
26 slopes in the Ecuadorian study region.

27

28 **1 Introduction**

29 Delineating flow path in a hillslope is still a challenging task (Bronstert, 1999; McDonnell et
30 al., 2007; Tetzlaff et al., 2008; Beven and Germann, 2013). Though a more complete
31 understanding in the partitioning of incoming water to surface runoff, lateral subsurface flow
32 components or percolation allows to better understand, for example, the impact of climate and
33 land use change on hydrological processes. Models are often used to test different rainfall-
34 runoff generation processes and the mixing of water in the soil (e.g. Kirkby, 1988; Weiler and
35 McDonnell, 2004). Due to the prevailing measurement techniques and therefore the available

datasets it has become common practice to base the validation of modeled hillslope flow processes on quantitative data on storage change. In the simplest case, system wide storage changes are monitored by discharge and groundwater level measurements or, on more intensively instrumented hillslopes, the storage change of individual soil compartments is monitored by soil moisture sensors. In the typical 2-D flow regime of a slope, such models bear the necessity not only to account for the vertical but also for the lateral movements of water within the soil (Bronstert, 1999). Quantitative data on storage change in this regard are only suitable to account for the actual change in soil water volume, but not to assess the source or flow direction. Knowing tracer compositions of relevant hydrological components along a hillslope allows to account for mixing processes and thereby to delineate the actual source of the incoming water. Over the years a number of artificial, e.g. fluorescence tracers like Uranine, and natural tracers, e.g. chloride or stable water isotopes, have emerged. While the application of the artificial tracers is rather limited in space and time (Leibundgut et al., 2011), the latter ones can be used over a wide range of scales (Barthold et al., 2011; Genereux and Hooper, 1999; Leibundgut et al., 2011; Muñoz-Villers and McDonnell, 2012; Soulsby et al., 2003). Stable water isotopes such as oxygen-18 (^{18}O) and hydrogen-2 (^{2}H) are integral parts of water molecules and consequently ideal tracers of water. Over the last decades isotope tracer studies have proven to provide reliable results on varying scales (chamber, plot, hillslope to catchment scale) and surface types (open water, bare soils, vegetated areas) to delineate or describe flow processes under field experimental or laboratory conditions (Garvelmann et al., 2012; Hsieh et al., 1998; Sklash et al., 1976; Vogel et al., 2010; Zimmermann et al., 1968).

Although the first 1d process orientated models to describe the dynamics of stable water isotope profiles for open water bodies (Craig and Gordon, 1965) and a bit later for soils (Zimmermann et al., 1968) have been developed as early as in the mid 1960's, fully distributed 2-D to 3-D hydrological tracer models benefitting from the additional information

62 to be gained by stable water isotopes are still in their early development stages (Davies et al.,
63 2013) or use strong simplifications of the flow processes (e.g. TAC^D using a kinematic wave
64 approach; Uhlenbrook et al., 2004). This can be attributed to the high number of interwoven
65 processes affecting the soil water isotope fluxes not only in the soil's liquid phase but also in
66 its vapor phase. The more process based 1d models (Braud et al., 2005; Haverd and Cuntz,
67 2010) therefore simultaneously solve the heat balance and the mass balance simultaneously
68 for the liquid and the vapor phase and are thereby describing the:

69 • convection and molecular diffusion in the liquid and vapor phase,
70 • equilibrium fractionation between liquid and vapor phase,
71 • fractionation due to evaporation, and
72 • non-fractionated flux due to percolation and transpiration.

73 To obtain and compute the data required to apply these kind of models beyond the plot scale
74 is still challenging. However, due to emerging measuring techniques the availability of
75 sufficient data becomes currently more realistic. Increasing computational power and
76 especially the cavity ring-down spectroscopy (CRDS) - a precise and cost effective method to
77 analyze the signature of stable water isotopes (Wheeler et al., 1998) - promise progress.

78 Hence, it is tempting to investigate the suitability of isotope tracers to delineate hydrological
79 flow paths using a more physical modeling approach. Recent research in this direction
80 includes the work of McMillan et al. (2012) and Hrachowitz et al. (2013) using chloride as a
81 tracer to study the fate of water in catchments in the Scottish Highlands. Even though some
82 processes affecting the soil water isotope transport are still represented in a simplified manner
83 or could be , due to their limited effect/importance of the respective process within the given
84 study site, omitted, this approach allows us to determine the potential of soil water isotope
85 modeling in catchment hydrology and highlight future need for research.

This study is conducted in a 75 km² montane rain forest catchment in south Ecuador, the upper part of the Rio San Francisco, which has been under investigation since 2007 (Bogner et al., 2014; Boy et al., 2008; Bücker et al., 2011; Crespo et al., 2012; Fleischbein et al., 2006; Goller et al., 2005; Timbe et al., 2014; Windhorst et al., 2013b). The findings of those studies (briefly synthesized in section 2.3) will a) ease the setup of chosen model, b) let us define suitable boundary conditions for the chosen modeling approach and c) serve as a reference for the delineated flow bath. The additional information from previous studies conducted in the study area, will therefore highlight the potential of this new model approach to delineate hydrological flow paths under natural conditions and support our preliminary hydrological process understanding retrieved from more classical methods conducted in the past.

Within this catchment we selected a hillslope with a distinct drainage area and nearly homogenous land-use and established an experimental sampling scheme to monitor the isotopic signatures of the soil water of three soil profiles using passive capillary fiberglass wick samplers (PCaps). Based on the proposed modeling approach a 2-D virtual hillslope representation of this hillslope was then implemented using the Catchment Modeling Framework (CMF; Kraft et al., 2011). Due to the necessity to mix the flows in accordance to the observed soil water isotope signatures we are confident, that the degree of certainty for the modeled flow path will be higher, than for conventional modeling approaches relying solely on quantitative information to evaluate the modeled data. Replacing the calibration target bears now the necessity to mix the right amount and signature of any given flow component, whereas the quantitative change only relies on the actual amount of water leaving or entering any given compartment. We will quantify the following flow components to disentangle the runoff generation processes: surface runoff, lateral subsurface flow in the vadose zone and percolation to groundwater. The lateral subsurface flow will be further subdivided into near surface lateral flow and deep lateral flow.

111 To validate the chosen modeling approach and assess our process understanding we tested the
112 following hypotheses:

113 I. Under the given environmental conditions - high precipitation and humidity -
114 (Bendix et al., 2008) and full vegetation cover (Dohnal et al., 2012; Vogel et al.,
115 2010) only non-fractionating and advective water transport of isotopes is relevant.
116 Gaseous advection and diffusive process in the gaseous as well as the liquid phase
117 and the enrichment due to evaporation are negligible; hence the stable water
118 isotopes behave like a conservative tracer.
119 II. Large shares of the soil water percolate to deeper horizons, thereby creating long
120 mean transit times (MTT) (Crespo et al., 2012; Timbe et al., 2014).
121 III. Due to the high saturated conductivities of the top soil layers the occurrence of
122 Hortonian overland flow is unlikely to have an important contribution to the
123 observed flows (Crespo et al., 2012)
124 IV. Fast near surface lateral flow contributes essentially to downhill water flows and
125 play a relevant role to understand the overall hydrological system (Bücker et al.,
126 2010).

127

128 **2 Materials and Methods**

129 **2.1 Study area**

130 The hillslope under investigation is located within the catchment of the Rio San Francisco in
131 South Ecuador (3°58'30"S, 79°4'25"W) at the eastern outskirts of the Andes and
132 encompasses an area of 75 km^2. Close to the continental divide the landscape generally
133 follows a continuous eastward decline towards the lowlands of the Amazon basin (Figure 1b).
134 Due to the high altitudes (1720-3155m a.s.l.), the deeply incised valleys (slopes are on

135 average 25°-40° over the entire watershed), the low population density and the partly
136 protected areas of the Podocarpus National Park, the human impact within the catchment is
137 relatively low. The southern flanks of the Rio San Francisco are covered by an almost pristine
138 tropical mountain cloud forest and lie mostly within the Podocarpus National Park. At lower
139 elevations the northern flanks have mostly been cleared by natural or slash-and-burn fires
140 during the last decades and are now partially used for extensive pasture (*Setaria sphacelata*
141 Schumach.), reforestation sites (*Pinus patula*), are covered by shrubs or invasive weeds
142 (especially tropical bracken fern; *Pteridium aquilinum* L.). The climate exhibits a strong
143 altitudinal gradient creating relatively low temperatures and high rainfall amounts (15.3°C
144 and 2000 mm a^{-1} at 1960 m a.s.l. to 9.5°C and >6000 mm a^{-1} at 3180 m a.s.l.) with the main
145 rainy season in the austral winter (Bendix et al., 2008). A comprehensive description of the
146 soils, climate, geology and land use has been presented by Beck et al. (2008), Bendix et al.
147 (2008) and Huwe et al. (2008).

148 **2.2 Experimental hillslope**

149 To test our understanding of hydrological processes within the study area we choose a
150 hillslope with a nearly homogenous land use (Figure 1). It is located on an extensive pasture
151 site with low intensity grazing by cows and dominated by *Setaria sphacelata*. *Setaria*
152 *sphacelata* is an introduced tropical C4 grass species that forms a dense tussock grassland
153 with a thick surface root mat (Rhoades et al., 2000). This grass is accustomed to high annual
154 rainfall intensities (>750 mm a^{-1}), has a low drought resistance and tolerates water logging to
155 a greater extent than other tropical grass types (Colman and Wilson, 1960; Hacker and Jones,
156 1969). The hillslope has a drainage area of 0.025 km², a hypothetical length of the subsurface
157 flow of 451 m and an elevation gradient of 157 m with an average slope of 19.2°. The soil
158 catena of the slope was recorded by Pürckhauer sampling and soil pits. To investigate the
159 passage of water through the hillslope a series of three wick sampler has been installed along
160 the line of subsurface flow.

Climate forcing data with an hourly resolution of precipitation, air temperature, irradiation, wind speed and relative humidity was collected by the nearby (400 m) climate station "ECSF" at similar elevation. Isotopic forcing data was collected manually for every rainfall event from Oct 2010 until Dec 2012 using a Ø25 cm funnel located in close proximity of the chosen hillslope at 1900 m a.s.l. (Timbe et al., 2014). To prevent any isotopic fractionation after the end of a single rainfall event (defined as a period of 30min without further rainfall) all samples where directly sealed with a lid and stored within a week in 2mL amber glass bottles for subsequent analysis of the isotopic signature as described in section 2.4.1 (all samples <2ml where discarded).

2.3 Current process understanding at the catchment scale

The catchment of the Rio San Francisco has been under investigation since 2007 (Bücker et al., 2011; Crespo et al., 2012; Timbe et al., 2014; Windhorst et al., 2013b) and was complemented by a number of studies on forested micro catchments (≈0.1 km²) within this catchment (Bogner et al., 2014; Boy et al., 2008; Fleischbein et al., 2006; Goller et al., 2005). Studies on both scales identify the similar hydrological processes to be active within the study area.

Studies on the micro scale (Boy et al., 2008; Goller et al., 2005), supported by solute data and end member mixing analysis at the meso scale (Bücker et al., 2011; Crespo et al., 2012), showed that fast 'organic horizon flow' in forested catchments dominates during discharge events, if the mineral soils are water saturated prior to the rainfall. Due to an abrupt change in saturated hydraulic conductivity (K_{sat}) between the organic (38.9 m d^{-1}) and the near-surface mineral layer (0.15 m d^{-1}) this 'organic horizon flow' can contribute up to 78% to the total discharge during storm events (Fleischbein et al., 2006; Goller et al., 2005). However, the overall importance of this 'organic horizon flow' is still disputable, because the rainfall intensity rarely gets close to such a high saturated hydraulic conductivity. In 95% of the

186 measured rainfall events between Jun 2010 and Oct 2012 the intensity was below 0.1 m d^{-1}
187 (≈4.1 mm h^{-1}) and was therefore 15 times lower than the saturated hydraulic conductivity of
188 the mineral soil layer below the organic layer under forest vegetation and around 30 times
189 lower than the saturated hydraulic conductivity of the top soil under pasture vegetation
190 (Zimmermann and Elsenbeer, 2008; Crespo et al., 2012). The same conclusion holds true for
191 the occurrence of surface runoff due to infiltration access on pasture (lacking a significant
192 organic layer). Solely based on rainfall intensities surface runoff is therefore relatively
193 unlikely to contribute to a larger extend in rainfall-runoff generation. The reported K_{sat} values
194 are based on measurements of 250 cm^3 undisturbed soil core samples vertically extracted
195 from the center of each respective layer. Due to the chosen sampling method and the limited
196 size of the soil cores the effective saturated hydraulic conductivity will be even higher and can
197 vary for the horizontal flow component. When and to which extent a subsurface saturated
198 prior the rainfall event would still trigger surface runoff on pastures therefore remains to be
199 investigated.

200 Bücker et al. (2010) and Timbe et al. (2014) could show that base flow on the other hand has
201 a rather large influence on the annual discharge volume across different land use types,
202 accounting for >70% and >85%, respectively. These findings are also supported by the long
203 mean transit time (MTT) of the base flow for different sub-catchments of the Rio San
204 Francisco in comparison to the fast runoff reaction times, varying according to Timbe et al.
205 (2014) between 2.1 and 3.9 years. Accordingly, the current findings confirm that the base
206 flow – originating from deeper mineral soil and bedrock layers– is dominating the overall
207 hydrological system in the study area (Crespo et al., 2012; Goller et al., 2005). Apart from this
208 dominating source of base flow, Bücker et al. (2010) identified near surface lateral flow as a
209 second component to be relevant for the generation of base flow for pasture sites.

2.4 Measurements

2.4.1 Passive capillary fiberglass wick samplers (PCaps)

We installed *passive capillary fiberglass wick samplers* (PCaps; short *wick samplers*, designed according to Mertens et al. (2007)) as soil water collectors at three locations along an altitudinal transects under pasture vegetation in three soil depths. PCaps maintain a fixed tension based on the type and length of wick (Mertens et al., 2007), require low maintenance and are most suitable to sample mobile soil water without altering its isotopic signature (Frisbee et al., 2010; Landon et al., 1999). We used woven and braided 3/8-inch fiberglass wicks (Amatex Co. Norristown, PA, US). 0.75 m of the 1.5 m wick was unraveled and placed over a 0.30 x 0.30 x 0.01 m square plastic plate, covered with fine grained parent soil material and then set in contact with the undisturbed soil.

Every collector was designed to sample water from three different soil depths (0.10, 0.25 and 0.40 m) with the same suction, all having the same sampling area of 0.09 m², wick type, hydraulic head of 0.3 m (vertical distance) and total wick length of 0.75 m. To simplify the collection of soil water the wick samplers drained into bottles placed inside a centralized tube with an inner diameter of 0.4 m and a depth of 1.0 m. To avoid any unnecessary alterations of the natural flow above the extraction area of the wick sampler the centralized tube was placed downhill and the plates where evenly spread uphill around the tube. A flexible silicon tube with a wall thickness of 5 mm was used to house the wick and to connect it to the 2 L sampling bottles storing the collected soil water. The silicon tube prevents evaporation and contamination of water flowing through the wick. Weekly bulk samples were collected over the period from Oct 2010 until Dec 2012 if the sample volume exceeded 2 mL. Soil water and the previously mentioned precipitation samples are analyzed using a cavity ring down spectrometer (CRDS) with a precision of 0.1 per mil for ^{18}O and 0.5 for ^{2}H (Picarro L1102-i, CA, US).

2.4.2 **Soil survey**

The basic soil and soil hydraulic properties for each distinct soil layer along the hillslope where investigated up to a depth of 2 m. Pürckhauer sampling for soil texture and succession of soil horizons was done every 25 m, while every 100 m soil pits were dug for sampling soil texture, soil water retention curves (pF-curves), porosity and succession of soil horizons. The results were grouped into 8 classes (Tab. 1) and assigned to the modeling mesh as shown in Figure 2. Retention curves (pF-curves) were represented by the *Van Genuchten-Mualem* function using the parameters α and n.

All soils developed from the same parent material (clay schist) and are classified as Haplic Cambisol with varying soil thickness. Soil thickness generally increased downhill varying between 0.8 m and 1.8 m in depressions. Clay illuviation was more pronounced in the upper part of the hillslope (higher gradient in clay content) indicating lower conductivities in deeper soil layers.

2.5 Modeling

2.5.1 The Catchment Modeling Framework (CMF)

The Catchment Modeling Framework (CMF) developed by Kraft et al. (2011) is a modular hydrological model based on the concept of finite volume method introduced by Qu and Duffy (2007). Within CMF those finite volumes (e.g. soil water storages, streams) are linked by a series of flow accounting equations (e.g. Richards or Darcy equation) to a one to three dimensional representation of the real world hydrological system. The flexible set up of CMF and the variety of available flow accounting equations allows customizing the setup as required in the presented study. In addition to the water fluxes, the advective movement of tracers within a given system can be accounted for by CMF, making this modeling framework especially suitable to be used in our tracer study (Kraft et al., 2010). Starting with Beven and Germann (1982) scientist over the last decades frequently argued that Richards equation like

flow accounting equation assuming a time invariant and well mixed homogenous flow of water through the soil pore space, similar to those currently implemented in CMF, are not suitable to account for preferential flow relevant for modeling tracer transport (Brooks et al., 2010; Germann et al., 2007; Hrachowitz et al., 2013; Stumpp and Maloszewski, 2010). Being developed for the quantitative representation of soil water flow this equations cannot distinguish between water stored in different soil compartments (namely the soil matrix and macro pores) and only artificially try to represent macropore flow e.g. by favoring high saturated conductivity values or misshaped conductivity curves controlling the flow of water between soil compartments. Even though the capabilities of CMF to account for preferential flow are still in the development phase (e.g. by following the dual permeability approach in the future) and are not accounted for in the presented setup, our setup will once more highlight potential draw backs of the modeling approaches relying on Richards equation while modeling tracer transport at the hillslope scale.

2.5.2 Setup of CMF

To govern the water fluxes within our system we used the following flow accounting equations: Manning equation for surface water flow; Richards equation for a full 2-D representation of the subsurface flow; Shuttleworth-Wallace modification (Shuttleworth and Wallace, 1985) of the Penman-Monteith method to control evaporation and transpiration; constant Dirichlet boundary conditions representing the groundwater table and the outlet of the system as a rectangular ditch with a depth of 1.5 m. The lower boundary condition is only applicable if groundwater table is >2 m below ground. Preliminary testing revealed that a discretization based on a constant vertical shift (5m) and alternating cell width increasing width depth (ranging from 1.25 cm to 83.75 cm) yielded the optimum model performance with regard to computing time and model quality. Based on 5 m contour lines (derived by local LIDAR measurements with a raster resolution of 1 m; using the Spatial Analyst package of ArcGis 10.1 from ESRI) this hillslope was further separated into 32 cells ranging in size

286 from 16.6 m² to 2,921.6 m² (Figure 1a). To account for small scale dynamics in the mixing
287 process of stable water isotopes and to be able to run the model with a satisfactory speed, two
288 different horizontal resolutions were used to discretize the each layer with depth. Layers
289 encompassing wick samplers and their upslope neighbor were run with a finer resolution of at
290 least 26 virtual soil layers increasing in thickness width depth (1x1.25 cm, 13 x 2.5 cm,
291 7 x 5 cm and 5 x 10-50 cm). All other cells were calculated with coarser resolution of at least
292 14 virtual soil layers (1 x 1.25 cm, 1 x 2.5 cm, 6 x 5 cm, 3 x 10 cm and 3 x 15-83.75 cm). In
293 case the delineated soil type changed within a soil layer it was further subdivided according to
294 Figure 2.

295 **2.5.3 Evapotranspiration**

296 Soil evaporation, evaporation of intercepted water and plant transpiration are calculated
297 separately using the sparse canopy evapotranspiration method by Shuttleworth and Wallace
298 (1985), in its modification by Federer et al. (2003) and Kraft et al. (2011). This approach
299 requires the following parameterizations: soil surface wetness dependent resistance to extract
300 water from the soil (r_{ss}), the plant type dependent bulk stomatal resistance to extract water
301 from the leaves (r_{sc}), the aerodynamic resistances parameters (r_{aa}, r_{as}, and r_{ac}) for sparse crops
302 as described by Shuttleworth and Gurney (1990) and Federer et al. (2003). Whereby r_{ac}
303 (Resistance Canopy Atmosphere) restricts the vapor movement between the leaves and the
304 zero plane displacement height and r_{as} (Resistance Soil Atmosphere) restricts the vapor
305 movement between the soil surface and the zero plane displacement height, which is the
306 height of the mean canopy flow (Shuttleworth and Wallace, 1985; Thom, 1972). The
307 aerodynamic resistances parameter r_{aa} refers to the resistance to move vapor between the zero
308 plane displacement height and the reference height at which the available measurements were
309 made. The necessary assumptions to parameterize the plant (*Setaria sphacelata*) and soil
310 dependent parameters of the Shuttleworth-Wallace equation using the assumptions made by
311 Federer et al. (2003) and Kraft et al. (2011) are listed in Tab. 2.

312 Furthermore, soil water extraction by evaporation is only affecting the top soil layer and soil
313 water extraction by transpiration is directly controlled by root distribution at a certain soil
314 depth. In accordance with field observations, we assumed an exponential decay of root mass
315 with depth, whereby 90 % of the total root mass is concentrated in the top 0.20 m.

316

317 **2.5.4 Calibration & Validation**

318 For calibration and validation purposes, we compared measured and modeled stable water
319 isotope signatures of ^{2}H and ^{18}O of the soil water at each depths of the each wick sampler
320 along the modeled hillslope. Hourly values of the modeled isotopic soil water signature were
321 aggregated to represent the mean isotopic composition in between measurements (≈7 days)
322 and are reported in per mil relative to the Vienna Standard Mean Ocean Water (VSMOW)
323 (Craig, 1961).

324 Literature and measured values for soil and plant parameters (Tab. 1 and Tab. 2) were used to
325 derive the initial values for the calibration process. The initial states for calibration were
326 retrieved by artificially running the model with those initial values for the first 2 years of the
327 available dataset (Tab. 3). The results of this pre-calibration run were used as a starting point
328 for all following calibration runs. A warm up period of 4 month (1.7.2010-31.10.10) preceded
329 the calibration period (1.11.2010-31.10.2011) to adjust the model to the new parameter set.
330 To simulate a wide range of possible flow conditions and limit the degrees of freedom for the
331 possible model realizations we selected K_{sat} and porosity for calibration, while the *Van*
332 *Genuchten-Mualem* parameters remained constant since measured pF curves where available.
333 Even though not all sensitive parameters of the Richards equation controlling the flow regime
334 where accounted for during the calibration process, we assume that the measured *Van*
335 *Genuchten-Mualem* parameters alpha and n are in the good agreement with the actual flow
336 characteristics of the soils. As typical for the application of the VanGenuchten - Mualem

337 approach the tortuosity/connectivity coefficient remained constant throughout all model runs
338 with a value of 0.5. Beside the 4 soil parameters shown in Tab. 1 and the upper and lower the
339 boundary conditions, only the 9 parameters of the Shuttleworth-Wallace equation Tab. 2 had
340 to be set prior to each model run. To further control the unknown lower boundary condition
341 and complement the calibration process, the suction induced by groundwater depth was
342 changed for each calibration run.

343 To increase the efficiency of the calibration runs and evenly explore the given parameter
344 space we used the Latin-Hyper cube method presented by McKay et al. (1979). The parameter
345 range of each variable was therefore subdivided into 10 strata and sampled once using
346 uniform distribution. All strata are then randomly matched to get the final parameter sets. A
347 total of 10^5 parameter sets were generated for calibration with varying values for K_{sat} and
348 porosity for all 8 soil types as well as different groundwater depths. An initial trial using 10^4
349 parameter sets was used to narrow down the parameter range as specified in Tab. 4 for K_{sat}
350 and porosity for all 8 soil types and to 0 m to 100 m for the applicable groundwater depths.
351 The performance of each parameter set was evaluated based on the goodness-of-fit criteria
352 Nash-Sutcliffe efficiency (NSE) and the coefficient of determination (R^2). In addition, the
353 bias was calculated as an indicator for any systematic or structural deviation of the model.

354 After the calibration the best performing ("behavioral") models according to a NSE>0.15, an
355 overall bias<±20.0 ‰ δ^2H and a coefficient of determination R^2>0.65, were used for the
356 validation period (Tab. 3) using the final states of the calibration period as initial values.

357 **3 Results and discussion**

358 **3.1 Model performance**

359 In order to quantify the flow processes we first validated the overall suitability of the chosen
360 model approach and the performance of the parameter sets. The parameter sets best

representing the isotope dynamics of δ^2H (as previously defined as best performing ("behavioral") parameter sets; same accounts for $\delta^{18}O$; results are not shown) during the calibration period, explained the observed variation to even a higher degree during the validation period (average NSE 0.19 for calibration versus 0.35 for validation).

The linear correlation between modeled and observed isotope dynamics of δ^2H, for the best performing parameter sets, were equally good during the calibration and validation period ($R^2 \approx 0.66$) (Tab. 5). The goodness-of-fit criteria for the single best performing parameter set ("best model fit") shows an R^2 of 0.84 and a NSE of 0.42.

Figure 3 depicts the measured and modeled temporal development of the soil water isotope profile along the studied hillslope as well as the δ^2H signature and amount of the incoming rainfall used to drive the model. The measured temporal delay of the incoming signal with depth and the general seasonal pattern of the δ^2H signal are captured by the model (Figure 3).

The bias was negative throughout all model realizations during calibration and validation (-15.90 (±0.11 SD) ‰ δ^2H and -16.93 (±0.34 SD) ‰ δ^2H respectively see Tab. 5). Even though the high bias indicates a structural insufficiency of the model, we are confident that this can be mostly attributed by the discrimination of evaporation processes at the soil-atmosphere interface and on the canopy.

Our first hypothesis, that evaporation in general plays only a minor role for the soil water isotope cycle under full vegetation, therefore needs to be reconsidered. Even though hypothesis I has previously been frequently used as an untested assumption for various models (e.g. Vogel et al., 2010; Dohnal et al., 2012) it is rarely scrutinized under natural conditions. A complete rejection of this hypothesis could therefore affect the interpretations in those studies and limit their applicability. However, further studies are needed to support these findings and before finally rejecting this hypothesis. The lateral mixing processes maybe

385 obscuring the observed near surface enrichment and the effect of preferential flow currently
386 not fully accounted for could further hinder the full interpretation of these findings. It still
387 holds true, that:

388 - the quantitative loss due to surface evaporation on areas with a high leaf area index is
389 more or less insignificant (accounting for 38 mm a^{-1} out of 1,896 mm a^{-1}; ≈2%; Figure 5),
390 - the isotopic enrichment due to evaporation for vegetated areas is considerably lower than
391 for non-vegetated areas, as previously shown by Dubbert et al. (2013), and
392 - high rainfall intensity constrains any near surface isotopic enrichment related to
393 evaporation (Hsieh et al., 1998).

394 However, our results indicate that the contribution of potential canopy evaporation
395 (accounting for 344 mm a^{-1} out of 1,896 mm a^{-1}; ≈18%; Figure 5) to enrich the canopy storage
396 and thereby potential throughfall (discriminating ^{18}O and ^{2}H resulting in more positive isotope
397 signatures) still could partially explain the observed bias.

398 Nevertheless we presume that fog drip, created by sieving bypassing clouds or radiation fog
399 frequently occurring in the study area Bendix et al. (2008), explains the majority of the
400 observed bias. Depending on the climatic processes generating the fog drip is typically
401 isotopically enriched compared to rainfall, due to different condensation temperatures (Scholl
402 et al., 2009). To get an impression for the magnitude of the possible bias due to throughfall
403 and fog drip compared to direct rainfall, we compare the observed bias with a study presented
404 by Liu et al. (2007) conducted in a tropical seasonal rain forest in China. They observed an
405 average enrichment of +5.5 ‰ $\delta^{2}H$ for throughfall and +45.3 ‰ $\delta^{2}H$ for fog drip compared
406 to rainfall. Even though the observed enrichment of fog drip and throughfall by Liu et al.
407 (2007) may not be as pronounced within our study area (Goller et al., 2005), the general
408 tendency could explain the modeled bias. According to Bendix et al. (2008) fog and cloud
409 water deposition within our study area contributes 121 mm a^{-1} to 210 mm a^{-1} at the respective

410 elevation. Assessing the actual amount fog drip for grass species like *Setaria sphacelata*
411 under natural conditions is challenging and has so far not been accounted for.

412 In case that further discrimination below the surface would substantially alter the isotope
413 signature, the bias would change continuously with depth. Any subsurface flow reaching wick
414 samplers at lower elevations would then further increase the bias. However, the negative bias
415 of -16.19 (±2.80 SD) ‰ δ^2H in all monitored top wick samplers during validation accounts
416 for most of the observed bias in the two deeper wick samplers amounting to
417 -17.32 (±2.47 SD) ‰ δ^2H. Thus we conclude that the bias is mainly a result of constrains
418 related to modeling surface processes, rather than subsurface ones.

419 Figure 4 shows the behavior of the chosen parameter sets for saturated hydraulic conductivity
420 and groundwater depth during calibration and validation. The parameter space allows us to
421 assess the range of suitable parameters and their sensitivity over a given parameter range.
422 During calibration the given parameter space could not be constrained to more precise values
423 for all parameters, which in this case should show a lower SD (Tab. 6) and narrower box plots
424 (Figure 4). Especially the K_{sat} values of the soil layers A1, A3 and B1-B3, the porosity for all
425 soil layers (not included in Figure 4) and the groundwater depth depict a low sensitive over
426 the entire calibration range (indicated by a high SD, wide box plot, and evenly scattered
427 points; Tab. 6 and Figure 4). In particular the low sensitivity of the model towards
428 groundwater depth seems surprising, but can be explained by the potentially low saturated
429 hydraulic conductivities of the lower soil layers C1 and C2 limiting the percolation into the
430 lower soil layers outside of the modeling domain. Even an extreme hydraulic potential,
431 induced by a deep groundwater body, can be limited by a low hydraulic conductivity. None
432 the less it noteworthy, that no model run without an active groundwater body as a lower
433 boundary condition (groundwater depth<2 m) results in a model performance with NSE>0
434 (Figure 4). With a groundwater depth above 2 m the boundary condition would serve as a

source of water with an undefined isotopic signal and prevent any percolation of water into deeper soil layers outside of the modeling domain. The results are therefore in alignment with the topography of the system indicating an active groundwater body deeper than 2 m and support our second hypothesis which we will further discuss in section 3.2. We identified several parameter combinations showing the same model performance, known as equifinality according to Beven and Freer (2001). The observed equifinality can partially be explained by counteracting effects of a decreasing K_{sat} and an increasing pore space, or that the water flow is restrained due to lower hydraulic conductivities at adjoining soil layers. Especially for deeper soil layers the interaction between surrounding layers makes it especially difficult to further constrain the given parameter range. Even though the parameter ranges for all behavioral model realizations are not so well confined, the small confidence intervals indicate a certain degree of robustness towards the predicted flows (Figure 3). Additional soil moisture measurements complementing the current setup in the future will allow us to put further confidence in this new approach and the drawn conclusions and allow us to directly compare different calibration targets (i.e. soil moisture vs. soil water isotopic signature).

Initial K_{sat} values based on literature values (see Tab. 1) deviate to a large extend from those derived through the calibration process. This is attributable to the occurrence of preferential flow within the macro pores (Bronstert and Plate, 1997) and the sampling method (PCaps) used to extract the soil water stored in the soil with a matrix potential up to 30 hPa (Landon et al., 1999). It becomes apparent that the mixing processes (based on dispersion and molecular diffusion) are not sufficient to equilibrate the isotope signature over the entire pore space (Landon et al., 1999; Šimůnek et al., 2003) and that the flow through the pore space is not homogenous. Thus the isotopic signature between the sampled pore media and the total modeled pore space differs (Brooks et al., 2010; Hrachowitz et al., 2013; McDonnell and Beven, 2014; McGlynn et al., 2002). The model tries to account for these effects by favoring high K_{sat} values during calibration (McDonnell and Beven, 2014; McGlynn et al., 2002).

461 Modeling soil water movement under such conditions should therefore be used with caution
462 for models based on Darcy-Richards equation which assume instantaneously homogeneous
463 mixed solutions and uniform flow. In line with the argumentation started by Beven and
464 Germann (1982) and refreshed in their recent paper Beven and Germann (2013) we therefore
465 stress the importance to account for preferential flow processes and overcome the limitation
466 of Darcy-Richards equation limiting the explanatory power of hydrological models predicting
467 water flow and solute/isotope transport in particular. Like Gerke (2006) and Šimůnek and van
468 Genuchten (2008) among others we therefore seek to implement a dual permeability approach
469 accounting for different flow patterns within the soil pore space (Gerke, 2006; Jarvis, 2007;
470 Šimůnek and van Genuchten, 2008; Vogel et al., 2000, 2006, 2010). In the style of existing 1-
471 Dmodels for soil water isotope transport presented by Braud et al. (2005) and Haverd and
472 Cuntz (2010) the inter-soil mixing processes by dispersion and molecular diffusion between
473 different soil pore space compartments shall be accounted for in the future. Based on the
474 presented findings this can now be extended towards the development and application of soil
475 water isotope models under natural conditions. To conclude, the results highlight the general
476 suitability of high resolution soil water isotope profiles to improve our understanding of
477 subsurface water flux separation implemented in current hillslope model applications and to
478 predict subsurface soil water movement.

479 **3.2 Modeled water fluxes**

480 Acknowledging the general suitability of the model to delineate the prevailing flow patterns,
481 we will now compare those to the current hydrological process understanding presented in the
482 introduction. Figure 5 depicts the water balance of the modeled hillslope based on all
483 behavioral model realizations, separating the amount of incoming precipitation into the main
484 flow components: surface runoff and subsurface flow directly entering the stream, percolation
485 to groundwater and evapotranspiration.

Evapotranspiration is further subdivided into transpiration and evaporation from the soil surface and the canopy, whereby evaporation from the canopy is designated as interception losses. Due to the small confidence intervals of the behavioral model runs (see Figure 3) the standard deviations of the model's flow components are relatively small (see Figure 5; standard deviation and mean value was computed without weighting the likelihood value).

The observed order of magnitude for evapotranspiration is in good agreement with previous values of 945 and 876 mm a^{-1} reported for tropical grasslands by Windhorst et al. (2013a) and Oke (1987), respectively. As previously mentioned the evaporation of 382 mm a^{-1} is dominated by interception losses accounting for 344 mm a^{-1}. Overall, these results support hypothesis II, which stated that a large share of the incoming precipitation is routed through the deeper soil layer and/or the groundwater body (here 49.7% or 942 mm a^{-1}) before it enters the stream. This also explains the long mean transit time of water of around 1.0 to 3.9 years (Crespo et al., 2012; Timbe et al., 2014) in comparison to the fast runoff reaction time. Well in agreement with our current process understanding and hypothesis III, we can further show that the occurrence of surface runoff (33 mm a^{-1}) due to Hortonian overland flow is less important. For the graphical representation the surface runoff has therefore been combined with subsurface flow (2 mm a^{-1}) to "surface runoff & subsurface flow", accounting in total for 35 mm a^{-1} (see Figure 5). A more heterogeneous picture can be depicted if we take a closer look at the flow processes along the studied hillslope and its soil profiles (Figure 6).

Vertical fluxes still dominate the flow of water (Figure 6b), but the near surface lateral flow components predicted by Bücker et al. (2010) become more evident (Figure 6a). Explained by the high saturated hydraulic conductivities in the top soil layers (Tab. 6 and Figure 4) up to 7.3 10^3 m^3 a^{-1} are transported lateral between cells in the top soil layer, referring to 15.6% of the total flow leaving the system per year. According to the model results deep lateral flow is minimal accounting only for <0.1% of the total flow. It only occurs on top of the deeper soil

511 horizons with low K_{sat} values. For all behavioral model realizations the groundwater level was
512 >2 m thereby limiting the direct contribution of subsurface flow (2 mm a^{-1}) to the tributary,
513 which had a hydraulic potential of only 1.5 m. Over the entire hillslope the importance of
514 overland flow remains below 3% (≈50 mm a^{-1}), of which a part is re-infiltrating, summing up
515 to total overland flow losses of around 2% at the hillslope scale (35 mm a^{-1}, Figure 5). These
516 results demonstrate the importance of near surface lateral flow and hence support hypothesis
517 IV.

518 **4 Conclusion**

519 These data and findings support and complement the existing process understanding mainly
520 gained by Goller et al. (2005), Fleischbein et al. (2006) Boy et al. (2008), Bücker et al.
521 (2010), Crespo et al. (2012) and Timbe et al. (2014) to a large extend. Moreover, it was
522 possible to quantify for the first time the relevance of near surface lateral flow generation. The
523 observed dominance of vertical percolation into the groundwater body and thereby the
524 importance of preferential flow seems to be quite common for humid tropical montane
525 regions and has recently been reported by Muñoz-Villers & McDonnell (2012) in a similar
526 environment.

527 Being aware of the rapid rainfall-runoff response of streams within the catchment of the Rio
528 San Francisco it has been questioned whether and how the system can store water for several
529 years and still release it within minutes. Throughout the last decades several studies have
530 observed similar hydrological behavior especially for steep humid montane regions (e.g.
531 McDonnell (1990) and Muñoz-Villers & McDonnell (2012)) and concepts have been
532 developed to explain this behavior: e.g. piston flow (McDonnell, 1990), kinematic waves
533 (Lighthill and Whitham, 1955), transmissivity feedback (Kendall et al., 1999). Due to the
534 limited depth of observations (max. depth 0.4 m) and the low overall influence of the lateral
535 flows a more exact evaluation of the fate of the percolated water is still not possible.

However, we are confident, that in combination with a suitable concept to account for the rapid mobilization of the percolated water into a tributary and experimental findings, further confining possible model realizations an improved version of the current approach, could further close the gap in our current process understanding.

Over decades hydrological models which are based on the Richards or Darcy equation (like the one we used), have been tuned to predict quantitative flow processes and mostly been validated using soil moisture data suitable to account for overall storage changes. Our results imply that doing this considerably well does not necessarily mean that the models actually transport the *right* water at the *right* time. Using tracer data to validate models as we did entails that those models now not only have to transport the correct amount but additionally the *right* water. Consequently, the relevance of the correct representation of uneven preferential flow through pipes or macropores, which is misleadingly compensated by high conductivities over the entire pore space within models based on the Richards or Darcy equation, becomes immense. Distinguishing between water flowing in different compartments (e.g. pipes, cracks and macro pores) of the soil is a key task to get a closer and more precise representation of the natural flow processes. Even though the chosen modeling structure currently lacks a sufficient robustness to be widely applicable it highlights the potential and future research directions for soil water isotope modeling.

Acknowledgments

The current study was conducted within the DFG Research Group FOR 816 “Biodiversity and sustainable management of a megadiverse mountain rain forest in south Ecuador” and the follow-up project PAK 825/3. The authors are very grateful for the funding supplied by the German Research Foundation DFG (BR2238/4-2 and BR 2238/14-1) and thank Thorsten Peters of the University of Erlangen for providing meteorological data.

References

Barthold, F.K., Tyralla, C., Schneider, K., Vaché, K.B., Frede, H.-G., Breuer, L., 2011. How many tracers do we need for end member mixing analysis (EMMA)? A sensitivity analysis. Water Resour. Res. 47, W08519. doi:10.1029/2011WR010604

Beck, E., Makeschin, F., Haubrich, F., Richter, M., Bendix, J., Valerezo, C., 2008. The Ecosystem (Reserva Biológica San Francisco), in: Beck, E., Bendix, J., Kottke, I., Makeschin, F., Mosandl, R. (Eds.), Gradients in a Tropical Mountain Ecosystem of Ecuador, Ecological Studies. Springer Berlin Heidelberg, pp. 1–13.

Bendix, J., Rollenbeck, R., Richter, M., Fabian, P., Emck, P., 2008. Climate, in: Beck, E., Bendix, J., Kottke, I., Makeschin, F., Mosandl, R. (Eds.), Gradients in a Tropical Mountain Ecosystem of Ecuador, Ecological Studies. Springer Berlin Heidelberg, pp. 63–73.

Bendix, J., Silva, B., Roos, K., Göttlicher, D.O., Rollenbeck, R., Nauß, T., Beck, E., 2010. Model parameterization to simulate and compare the PAR absorption potential of two competing plant species. Int. J. Biometeorol. 54, 283–295. doi:10.1007/s00484-009-0279-3

Beven, K., Germann, P., 1982. Macropores and water flow in soils. Water Resour. Res. 18, 1311–1325. doi:10.1029/WR018i005p01311

Beven, K., Germann, P., 2013. Macropores and water flow in soils revisited. Water Resour. Res. 49, 3071–3092. doi:10.1002/wrcr.20156

Bogner, C., Bauer, F., Trancón y Widemann, B., Viñan, P., Balcazar, L., Huwe, B., 2014. Quantifying the morphology of flow patterns in landslide-affected and unaffected soils. J. Hydrol. 511, 460–473. doi:10.1016/j.jhydrol.2014.01.063

Boy, J., Valarezo, C., Wilcke, W., 2008. Water flow paths in soil control element exports in an Andean tropical montane forest. Eur. J. Soil Sci. 59, 1209–1227. doi:10.1111/j.1365-2389.2008.01063.x

Braud, I., Bariac, T., Gaudet, J.P., Vauclin, M., 2005. SiSPAT-Isotope, a coupled heat, water and stable isotope (HDO and H218O) transport model for bare soil. Part I. Model description and first verifications. J. Hydrol. 309, 277–300. doi:10.1016/j.jhydrol.2004.12.013

Bronstert, A., 1999. Capabilities and limitations of detailed hillslope hydrological modelling. Hydrol. Process. 13, 21–48. doi:10.1002/(SICI)1099-1085(199901)13:1<21::AID-HYP702>3.0.CO;2-4

595 Bronstert, A., Plate, E.J., 1997. Modelling of runoff generation and soil moisture dynamics for
596 hillslopes and micro-catchments. J. Hydrol. 198, 177–195. doi:10.1016/S0022-
597 1694(96)03306-9
598 Brooks, J.R., Barnard, H.R., Coulombe, R., McDonnell, J.J., 2010. Ecohydrologic separation
599 of water between trees and streams in a Mediterranean climate. Nat. Geosci. 3, 100–
600 104. doi:10.1038/ngeo722
601 Bücker, A., Crespo, P., Frede, H.-G., Breuer, L., 2011. Solute behaviour and export rates in
602 neotropical montane catchments under different land-uses. J. Trop. Ecol. 27, 305–317.
603 doi:10.1017/S0266467410000787
604 Bücker, A., Crespo, P., Frede, H.-G., Vaché, K., Cisneros, F., Breuer, L., 2010. Identifying
605 Controls on Water Chemistry of Tropical Cloud Forest Catchments: Combining
606 Descriptive Approaches and Multivariate Analysis. Aquat. Geochem. 16, 127–149.
607 doi:10.1007/s10498-009-9073-4
608 Colman, R.L., Wilson, G.P.M., 1960. The Effect of Floods on Pasture Plants. Agric. Gaz.
609 NSW 71, 337–347.
610 Craig, H., 1961. Standard for Reporting Concentrations of Deuterium and Oxygen-18 in
611 Natural Waters. Science 133, 1833–1834. doi:10.1126/science.133.3467.1833
612 Craig, H., Gordon, L.I., 1965. Deuterium and oxygen 18 variations in the ocean and the
613 marine atmosphere, in: Tongiogi, E. (Ed.), Proceedings of the Conference on the
614 Stable Isotopes in Oceanographic Studies and Paleotemperatures. Lishi e F., Pisa,
615 Spoleto, Italy, pp. 9–130.
616 Crespo, P., Bücker, A., Feyen, J., Vaché, K.B., Frede, H.-G., Breuer, L., 2012. Preliminary
617 evaluation of the runoff processes in a remote montane cloud forest basin using
618 Mixing Model Analysis and Mean Transit Time. Hydrol. Process. 26, 3896–3910.
619 doi:10.1002/hyp.8382
620 Davies, J., Beven, K., Rodhe, A., Nyberg, L., Bishop, K., 2013. Integrated modeling of flow
621 and residence times at the catchment scale with multiple interacting pathways. Water
622 Resour. Res. 49, 4738–4750. doi:10.1002/wrcr.20377
623 Dohnal, M., Vogel, T., Šanda, M., Jelínková, V., 2012. Uncertainty Analysis of a Dual-
624 Continuum Model Used to Simulate Subsurface Hillslope Runoff Involving Oxygen-
625 18 as Natural Tracer. J. Hydrol. Hydromech. 60, 194–205. doi:10.2478/v10098-012-
626 0017-0
627 Dubbert, M., Cuntz, M., Piayda, A., Maguás, C., Werner, C., 2013. Partitioning
628 evapotranspiration – Testing the Craig and Gordon model with field measurements of
629 oxygen isotope ratios of evaporative fluxes. J. Hydrol. 496, 142–153.
630 doi:10.1016/j.jhydrol.2013.05.033
631 Federer, C.A., Vörösmarty, C., Fekete, B., 2003. Sensitivity of Annual Evaporation to Soil
632 and Root Properties in Two Models of Contrasting Complexity. J. Hydrometeorol. 4,
633 1276–1290. doi:10.1175/1525-7541(2003)004<1276:SOAETS>2.0.CO;2
634 Fleischbein, K., Wilcke, W., Valarezo, C., Zech, W., Knoblich, K., 2006. Water budgets of
635 three small catchments under montane forest in Ecuador: experimental and modelling
636 approach. Hydrol. Process. 20, 2491–2507. doi:10.1002/hyp.6212
637 Frisbee, M.D., Phillips, F.M., Campbell, A.R., Hendrickx, J.M.H., 2010. Modified passive
638 capillary samplers for collecting samples of snowmelt infiltration for stable isotope
639 analysis in remote, seasonally inaccessible watersheds 1: laboratory evaluation.
640 Hydrol. Process. 24, 825–833. doi:10.1002/hyp.7523
641 Garvelmann, J., Külls, C., Weiler, M., 2012. A porewater-based stable isotope approach for
642 the investigation of subsurface hydrological processes. Hydrol Earth Syst Sci 16, 631–
643 640. doi:10.5194/hess-16-631-2012

644 Genereux, D.P., Hooper, R.P., 1999. Oxygen and hydrogen isotopes in rainfall-runoff studies,
645 in: Kendall, C., McDonnell, J.J. (Eds.), Isotope Tracers in Catchment Hydrology.
646 Elsevier, pp. 319–346.
647 Gerke, H.H., 2006. Preferential flow descriptions for structured soils. J. Plant Nutr. Soil Sci.
648 169, 382–400. doi:10.1002/jpln.200521955
649 Germann, P., Helbling, A., Vadilonga, T., 2007. Rivulet Approach to Rates of Preferential
650 Infiltration. Vadose Zone J. 6, 207. doi:10.2136/vzj2006.0115
651 Goller, R., Wilcke, W., Leng, M.J., Tobschall, H.J., Wagner, K., Valarezo, C., Zech, W.,
652 2005. Tracing water paths through small catchments under a tropical montane rain
653 forest in south Ecuador by an oxygen isotope approach. J. Hydrol. 308, 67–80.
654 doi:10.1016/j.jhydrol.2004.10.022
655 Hacker, J.B., Jones, R.J., 1969. The Setaria sphacelata complex - a review. Trop. Grassl. 3,
656 13–34.
657 Haverd, V., Cuntz, M., 2010. Soil–Litter–Iso: A one-dimensional model for coupled transport
658 of heat, water and stable isotopes in soil with a litter layer and root extraction. J.
659 Hydrol. 388, 438–455. doi:10.1016/j.jhydrol.2010.05.029
660 Hrachowitz, M., Savenije, H., Bogaard, T.A., Tetzlaff, D., Soulsby, C., 2013. What can flux
661 tracking teach us about water age distribution patterns and their temporal dynamics?
662 Hydrol Earth Syst Sci 17, 533–564. doi:10.5194/hess-17-533-2013
663 Hsieh, J.C.., Chadwick, O.A., Kelly, E.F., Savin, S.M., 1998. Oxygen isotopic composition of
664 soil water: Quantifying evaporation and transpiration. Geoderma 82, 269–293.
665 doi:10.1016/S0016-7061(97)00105-5
666 Hunter, J.D., 2007. Matplotlib: A 2D Graphics Environment. Comput. Sci. Eng. 9, 90–95.
667 doi:10.1109/MCSE.2007.55
668 Huwe, B., Zimmermann, B., Zeilinger, J., Quizhpe, M., Elsenbeer, H., 2008. Gradients and
669 Patterns of Soil Physical Parameters at Local, Field and Catchment Scales, in: Beck,
670 E., Bendix, J., Kottke, I., Makeschin, F., Mosandl, R. (Eds.), Gradients in a Tropical
671 Mountain Ecosystem of Ecuador, Ecological Studies. Springer Berlin Heidelberg, pp.
672 375–386.
673 Jarvis, N.J., 2007. A review of non-equilibrium water flow and solute transport in soil
674 macropores: principles, controlling factors and consequences for water quality. Eur. J.
675 Soil Sci. 58, 523–546. doi:10.1111/j.1365-2389.2007.00915.x
676 Kendall, K.A., Shanley, J.B., McDonnell, J.J., 1999. A hydrometric and geochemical
677 approach to test the transmissivity feedback hypothesis during snowmelt. J. Hydrol.
678 219, 188–205. doi:10.1016/S0022-1694(99)00059-1
679 Kirkby, M., 1988. Hillslope runoff processes and models. J. Hydrol. 100, 315–339.
680 doi:10.1016/0022-1694(88)90190-4
681 Körner, C., Scheel, J., Bauer, H., 1979. Maximum leaf diffusive conductance in vascular
682 plants. Photosynthetica 13, 45–82.
683 Kraft, P., Multsch, S., Vaché, K.B., Frede, H.-G., Breuer, L., 2010. Using Python as a
684 coupling platform for integrated catchment models. Adv. Geosci. 27, 51–56.
685 doi:10.5194/adgeo-27-51-2010
686 Kraft, P., Vaché, K.B., Frede, H.-G., Breuer, L., 2011. CMF: A Hydrological Programming
687 Language Extension For Integrated Catchment Models. Environ. Model. Softw. 26,
688 828–830. doi:10.1016/j.envsoft.2010.12.009
689 Landon, M.K., Delin, G.N., Komor, S.C., Regan, C.P., 1999. Comparison of the stable-
690 isotopic composition of soil water collected from suction lysimeters, wick samplers,
691 and cores in a sandy unsaturated zone. J. Hydrol. 224, 45–54. doi:10.1016/S0022-
692 1694(99)00120-1
693 Leibundgut, C., Maloszewski, P., Külls, C., 2011. Tracers in Hydrology. John Wiley & Sons,
694 Chichester, UK.

695 Lighthill, M.J., Whitham, G.B., 1955. On Kinematic Waves. II. A Theory of Traffic Flow on
696 Long Crowded Roads. Proc. R. Soc. Lond. Ser. Math. Phys. Sci. 229, 317–345.
697 doi:10.1098/rspa.1955.0089
698 Liu, W.J., Liu, W.Y., Li, P.J., Gao, L., Shen, Y.X., Wang, P.Y., Zhang, Y.P., Li, H.M., 2007.
699 Using stable isotopes to determine sources of fog drip in a tropical seasonal rain forest
700 of Xishuangbanna, SW China. Agric. For. Meteorol. 143, 80–91.
701 doi:10.1016/j.agrformet.2006.11.009
702 McDonnell, J.J., 1990. A Rationale for Old Water Discharge Through Macropores in a Steep,
703 Humid Catchment. Water Resour. Res. 26, 2821–2832.
704 doi:10.1029/WR026i011p02821
705 McDonnell, J.J., Beven, K., 2014. Debates—The future of hydrological sciences: A
706 (common) path forward? A call to action aimed at understanding velocities, celerities
707 and residence time distributions of the headwater hydrograph. Water Resour. Res. 50,
708 5342–5350. doi:10.1002/2013WR015141
709 McDonnell, J.J., Sivapalan, M., Vaché, K., Dunn, S., Grant, G., Haggerty, R., Hinz, C.,
710 Hooper, R., Kirchner, J., Roderick, M.L., Selker, J., Weiler, M., 2007. Moving beyond
711 heterogeneity and process complexity: A new vision for watershed hydrology. Water
712 Resour. Res. 43, W07301. doi:10.1029/2006WR005467
713 McGlynn, B.L., McDonnel, J.J., Brammer, D.D., 2002. A review of the evolving perceptual
714 model of hillslope flowpaths at the Maimai catchments, New Zealand. J. Hydrol. 257,
715 1–26. doi:10.1016/S0022-1694(01)00559-5
716 McKay, M.D., Beckman, R.J., Conover, W.J., 1979. A Comparison of Three Methods for
717 Selecting Values of Input Variables in the Analysis of Output from a Computer Code.
718 Technometrics 21, 239–245. doi:10.2307/1268522
719 McMillan, H., Tetzlaff, D., Clark, M., Soulsby, C., 2012. Do time-variable tracers aid the
720 evaluation of hydrological model structure? A multimodel approach. Water Resour.
721 Res. 48, W05501. doi:10.1029/2011WR011688
722 Mertens, J., Diels, J., Feyen, J., Vanderborght, J., 2007. Numerical analysis of Passive
723 Capillary Wick Samplers prior to field installation. Soil Sci. Soc. Am. J. 71, 35–42.
724 doi:10.2136/sssaj2006.0106
725 Muñoz-Villers, L.E., McDonnell, J.J., 2012. Runoff generation in a steep, tropical montane
726 cloud forest catchment on permeable volcanic substrate. Water Resour. Res. 48,
727 W09528. doi:10.1029/2011WR011316
728 Oke, T.R., 1987. Boundary Layer Climates, 2nd ed. Methuen, London, UK.
729 Qu, Y., Duffy, C.J., 2007. A semidiscrete finite volume formulation for multiprocess
730 watershed simulation. Water Resour. Res. 43, W08419. doi:10.1029/2006WR005752
731 Rhoades, C.C., Eckert, G.E., Coleman, D.C., 2000. Soil carbon differences among forest,
732 agriculture, and secondary vegetation in lower montane Ecuador. Ecol. Appl. 10, 497–
733 505. doi:10.1890/1051-0761(2000)010[0497:SCDAFA]2.0.CO;2
734 Scholl, M.A., Shanley, J.B., Zegarra, J.P., Coplen, T.B., 2009. The stable isotope amount
735 effect: New insights from NEXRAD echo tops, Luquillo Mountains, Puerto Rico.
736 Water Resour. Res. 45, W12407. doi:10.1029/2008WR007515
737 Shuttleworth, W.J., Gurney, R.J., 1990. The theoretical relationship between foliage
738 temperature and canopy resistance in sparse crops. Q. J. R. Meteorol. Soc. 116, 497–
739 519. doi:10.1002/qj.49711649213
740 Shuttleworth, W.J., Wallace, J.S., 1985. Evaporation from sparse crops-an energy
741 combination theory. Q. J. R. Meteorol. Soc. 111, 839–855.
742 doi:10.1002/qj.49711146910
743 Šimůnek, J., Jarvis, N.J., van Genuchten, M.T., Gärdenäs, A., 2003. Review and comparison
744 of models for describing non-equilibrium and preferential flow and transport in the
745 vadose zone. J. Hydrol. 272, 14–35. doi:10.1016/S0022-1694(02)00252-4

Šimůnek, J., van Genuchten, M.T., 2008. Modeling Nonequilibrium Flow and Transport Processes Using HYDRUS. Vadose Zone J. 7, 782–797. doi:10.2136/vzj2007.0074

Sklash, M.G., Farvolden, R.N., Fritz, P., 1976. A conceptual model of watershed response to rainfall, developed through the use of oxygen-18 as a natural tracer. Can. J. Earth Sci. 13, 271–283. doi:10.1139/e76-029

Soulsby, C., Rodgers, P., Smart, R., Dawson, J., Dunn, S., 2003. A tracer-based assessment of hydrological pathways at different spatial scales in a mesoscale Scottish catchment. Hydrol. Process. 17, 759–777. doi:10.1002/hyp.1163

Stumpp, C., Maloszewski, P., 2010. Quantification of preferential flow and flow heterogeneities in an unsaturated soil planted with different crops using the environmental isotope δ18O. J. Hydrol. 394, 407–415. doi:10.1016/j.jhydrol.2010.09.014

Tetzlaff, D., McDonnell, J.J., Uhlenbrook, S., McGuire, K.J., Bogaart, P.W., Naef, F., Baird, A.J., Dunn, S.M., Soulsby, C., 2008. Conceptualizing catchment processes: simply too complex? Hydrol. Process. 22, 1727–1730. doi:10.1002/hyp.7069

Thom, A.S., 1972. Momentum, mass and heat exchange of vegetation. Q. J. R. Meteorol. Soc. 98, 124–134. doi:10.1002/qj.49709841510

Timbe, E., Windhorst, D., Crespo, P., Frede, H.-G., Feyen, J., Breuer, L., 2014. Understanding uncertainties when inferring mean transit times of water trough tracer-based lumped-parameter models in Andean tropical montane cloud forest catchments. Hydrol. Earth Syst. Sci. 18, 1503–1523. doi:10.5194/hess-18-1503-2014

Uhlenbrook, S., Roser, S., Tilch, N., 2004. Hydrological process representation at the meso-scale: the potential of a distributed, conceptual catchment model. J. Hydrol. 291, 278–296. doi:10.1016/j.jhydrol.2003.12.038

Vogel, H.-J., Cousin, I., Ippisch, O., Bastian, P., 2006. The dominant role of structure for solute transport in soil: experimental evidence and modelling of structure and transport in a field experiment. Hydrol Earth Syst Sci 10, 495–506. doi:10.5194/hess-10-495-2006

Vogel, T., Gerke, H.H., Zhang, R., Van Genuchten, M.T., 2000. Modeling flow and transport in a two-dimensional dual-permeability system with spatially variable hydraulic properties. J. Hydrol. 238, 78–89. doi:10.1016/S0022-1694(00)00327-9

Vogel, T., Sanda, M., Dusek, J., Dohnal, M., Votrubova, J., 2010. Using Oxygen-18 to Study the Role of Preferential Flow in the Formation of Hillslope Runoff. Vadose Zone J. 9, 252–259. doi:10.2136/vzj2009.0066

Weiler, M., McDonnell, J., 2004. Virtual experiments: a new approach for improving process conceptualization in hillslope hydrology. J. Hydrol. 285, 3–18. doi:10.1016/S0022-1694(03)00271-3

Wheeler, M.D., Newman, S.M., Orr-Ewing, A.J., Ashfold, M.N.R., 1998. Cavity ring-down spectroscopy. J. Chem. Soc. Faraday Trans. 94, 337–351. doi:10.1039/A707686J

Windhorst, D., Brenner, S., Peters, T., Meyer, H., Thies, B., Bendix, J., Frede, H.-G., Breuer, L., 2013a. Impacts of Local Land-Use Change on Climate and Hydrology, in: Bendix, J., Beck, E., Bräuning, A., Makeschin, F., Mosandl, R., Scheu, S., Wilcke, W. (Eds.), Ecosystem Services, Biodiversity and Environmental Change in a Tropical Mountain Ecosystem of South Ecuador, Ecological Studies Vol. 221. Springer, Berlin, Heidelberg, New York, pp. 275–286.

Windhorst, D., Waltz, T., Timbe, E., Frede, H.-G., Breuer, L., 2013b. Impact of elevation and weather patterns on the isotopic composition of precipitation in a tropical montane rainforest. Hydrol. Earth Syst. Sci. 17, 409–419. doi:10.5194/hess-17-409-2013

Zimmermann, B., Elsenbeer, H., 2008. Spatial and temporal variability of soil saturated hydraulic conductivity in gradients of disturbance. J. Hydrol. 361, 78–95. doi:10.1016/j.jhydrol.2008.07.027

797 Zimmermann, U., Ehhalt, D., Muennich, K.O., 1968. Soil-Water Movement and
798 Evapotranspiration: Changes in the Isotopic Composition of the Water., in: Isotopes in
799 Hydrology. International Atomic Energy Agency, Vienna, pp. 567–585.
800
801

802 **Tables**

803 **Tab. 1 Soil physical parameters**

Soil code	Texture			Porosity	K_{sat}*	*Van Genuchten-Mualem* Parameters	
	Clay [%]	Sand [%]	Silt [%]	[%]	[m/d]	α	n
A1 & A1 top	34	17	49	81	0.324	0.641	1.16
A2 & A2 top	19	33	49	63	0.324	0.352	1.13
A3 & A3 top	15	34	51	74	0.324	0.221	1.24
B1	8	16	76	66	0.228	1.046	1.19
B2	15	34	51	59	0.228	0.145	1.13
B3	11	18	70	58	0.228	0.152	1.16
C1	15	45	40	55	0.026	0.023	1.12
C2	45	20	35	47	0.026	0.004	1.17

*K_{sat} values are based on values taken within the proximity of the hillslope under similar land use by Crespo et al. (2012) and Zimmermann and Elsenbeer (2008).

804

805 **Tab. 2 Plant (*Setaria sphacelata*) and soil dependent parameters used for the Shuttleworth-Wallace equation**

Parameter	Symbol	Value	Unit	Used to calculate	Source
Potential soil surface resistance	$r_{ss\ pot}$	500	s m^{-1}	r_{ss}	Federer et al.(2003)
Max. stomatal conductivity or max. leaf conductance	g_{max}	270	s m^{-1}	r_{sc}	Körner et al. (1979)
Leaf area index	LAI	3.7	m^2 m^{-2}	r_{sc}	Bendix et al. (2010)
Canopy height	h	0.2	m	r_{aa}, r_{ac} & r_{as}	Estimate based on hand measurements
Representative leaf width	w	0.015	m	r_{ac}	
Extinction coefficient for photosynthetically active radiation in the canopy	CR	70	%	r_{sc}	Federer et al.(2003)
Canopy storage capacity	-	0.15	mm LAI^{-1}	Interception	Federer et al.(2003)
Canopy closure	-	90	%	Throughfall	Estimate based on image evaluation
Albedo	alb	11,7	%	Net radiation	Bendix et al. (2010)

806

807

808 **Tab. 3 Modeling periods**

Description	Period		Duration [days]
	Start	End	
Initial states	1 July 2010	30 June 2012	730
Warm up period	1 July 2010	31 October 2010	122
Calibration period	1 November 2010	31 October 2011	364
Validation period	1 November 2011	31 October 2012	365

809

810 **Tab. 4 Soil parameter ranges for the Monte Carlo simulations (assuming uniform distribution for each parameter).**

Soil code	K_{sat} [m d^{-1}]		Porosity [m^3 m^{-3}]	
	Min.	Max.	Min.	Max.
A1-3 top	0.001	35	0.3	0.9
A1-3	0.001	30	0.3	0.9
B1-3	0.001	12	0.1	0.8
C1-2	0.001	8	0.1	0.8

811

812 **Tab. 5 Model performance during calibration and validation for all behavioral model runs (based on all calibration**
813 **runs with NSE> 0.15, bias< ± 20.0 ‰ δ^2H and $R^2 > 0.65$). Best modeled fit based on NSE.**

	Calibration 2010-2011		Validation 2011-2012		Best modeled fit
	Mean	SD	Mean	SD	
NSE	0.19	0.008	0.35	0.029	0.42
R^2	0.67	0.008	0.66	0.020	0.84
Bias	-15.90	0.113	-16.93	0.344	-16.16

814

Tab. 6 Parameter ranges used for validation (all calibration runs with NSE>0.15, bias<±20.0 ‰ δ^2H and R^2> 0.65) and parameter set for the best modeled fit based on NSE.

	Mean	SD	Best modeled fit
K_{sat} [m d^{-1}]			
A1 top	21.8	5.8	20.4
A2 top	11.0	2.3	12.6
A3 top	25.6	6.3	29.6
A1	11.7	6.6	13.5
A2	7.4	2.8	8.9
A3	15.7	6.4	15.3
B1	4.0	2.4	4.0
B2	5.2	3.2	10.5
B3	4.6	2.2	2.5
C1	1.3	1.2	0.6
C2	1.7	1.4	0.1
Porosity [m^3 m^{-3}]			
A1 top	0.54	0.08	0.44
A2 top	0.56	0.09	0.44
A3 top	0.66	0.09	0.53
A1	0.55	0.08	0.42
A2	0.55	0.09	0.46
A3	0.65	0.09	0.74
B1	0.34	0.09	0.31
B2	0.64	0.09	0.54
B3	0.75	0.09	0.70
C1	0.54	0.09	0.41
C2	0.55	0.09	0.67
Groundwater depth [m]			
	50.5	28.6	76.5

Figures

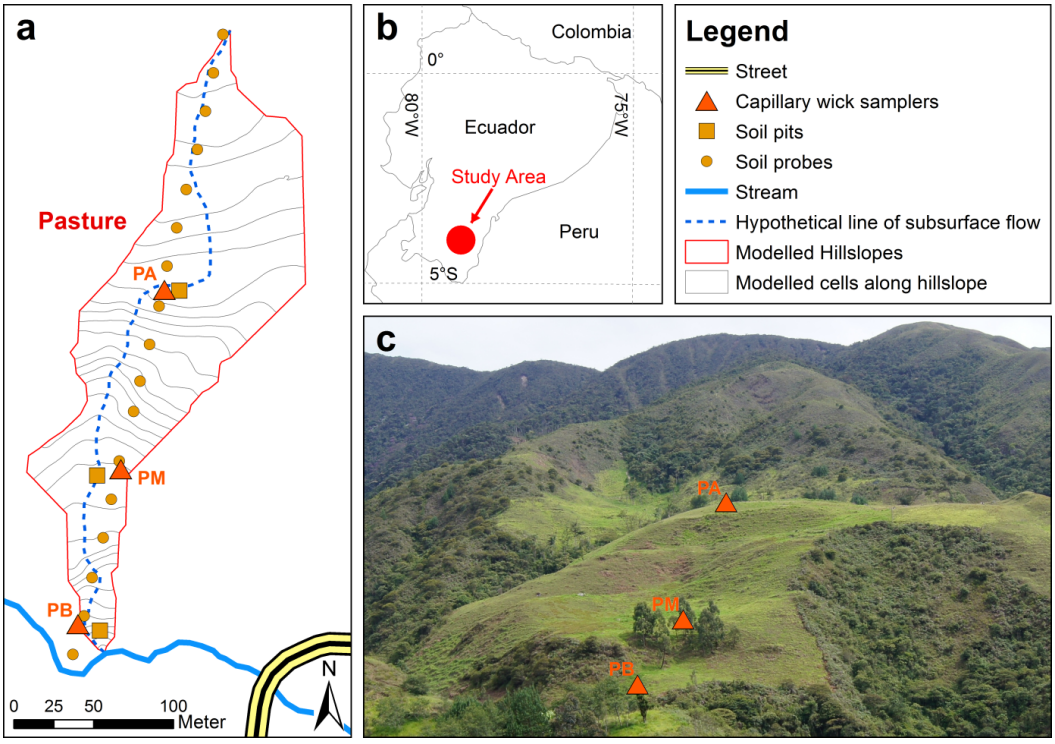

Figure 1 a) Outline of the modeled hillslope and its virtual discretization into cells. b) Location of the study area within Ecuador c) Photograph showing the Location of the wick samplers (P = Pasture and B = bajo/lower level, M = medio/middle level, A = alto/top level sampler).

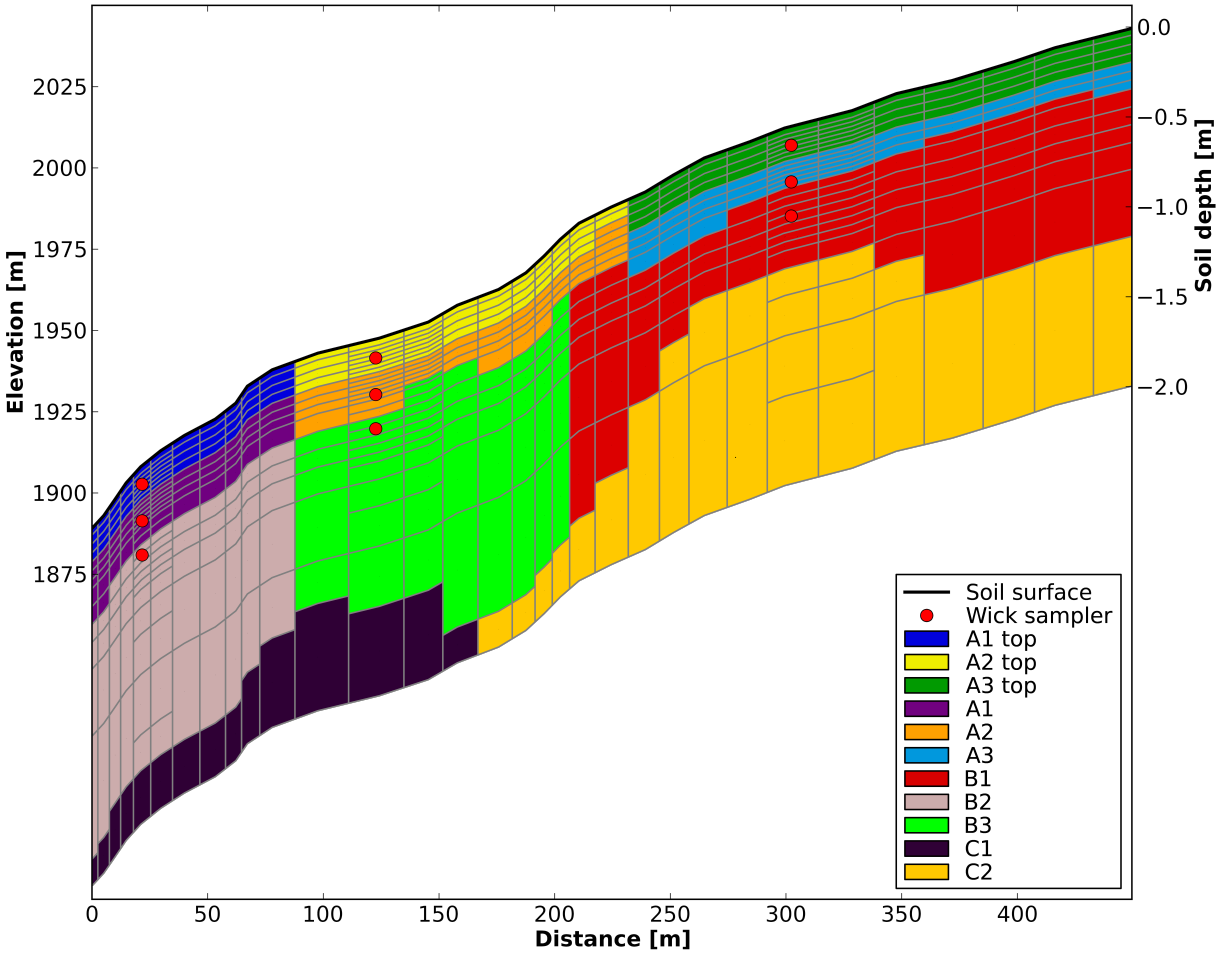

824

825 **Figure 2 Elevation profile (top black line, left ordinate), succession of soil layer types (color plate) and soil depths**
826 **assigned to the modeling grid (right ordinate).**

827

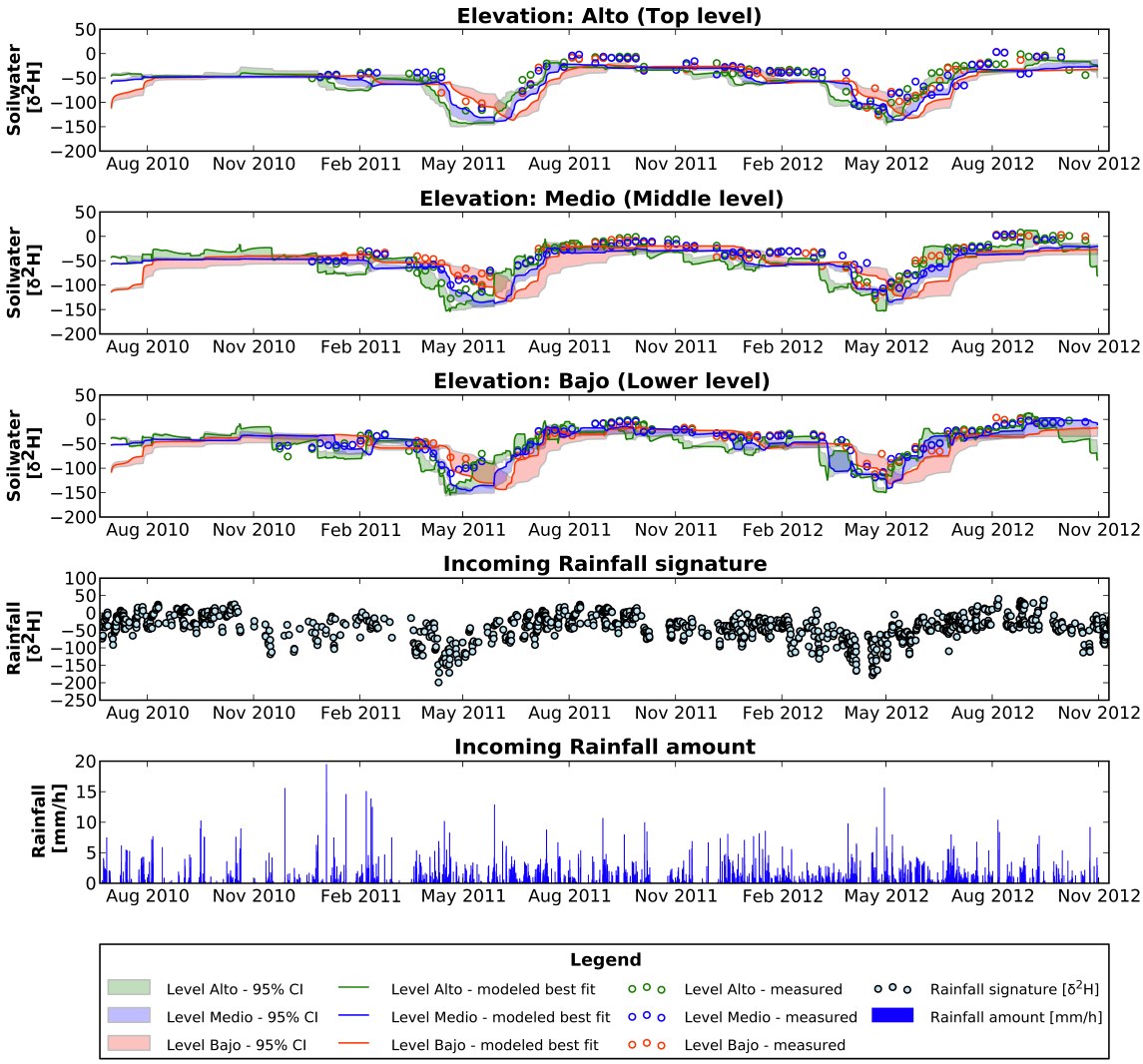

828

829 **Figure 3 Time series of soil water isotope signatures (Top panels 1-3 for each elevation) for all behavioral model runs**
830 **with: NSE> 0.15, bias<±20.0 ‰ δ^2H and R^2>0.65 showing the 95% confidence interval (CI; transparent**
831 **areas) and best modeled fit (solid line) vs. measured values (circles) at all 3 elevations (2,010, 1,949 and**
832 **1,904 m a.s.l.) and soil depths below ground (0.10, 0.25 and 0.40 m). Bottom panels 4 and 5, isotopic**
833 **signature and rainfall amount, respectively.**

834

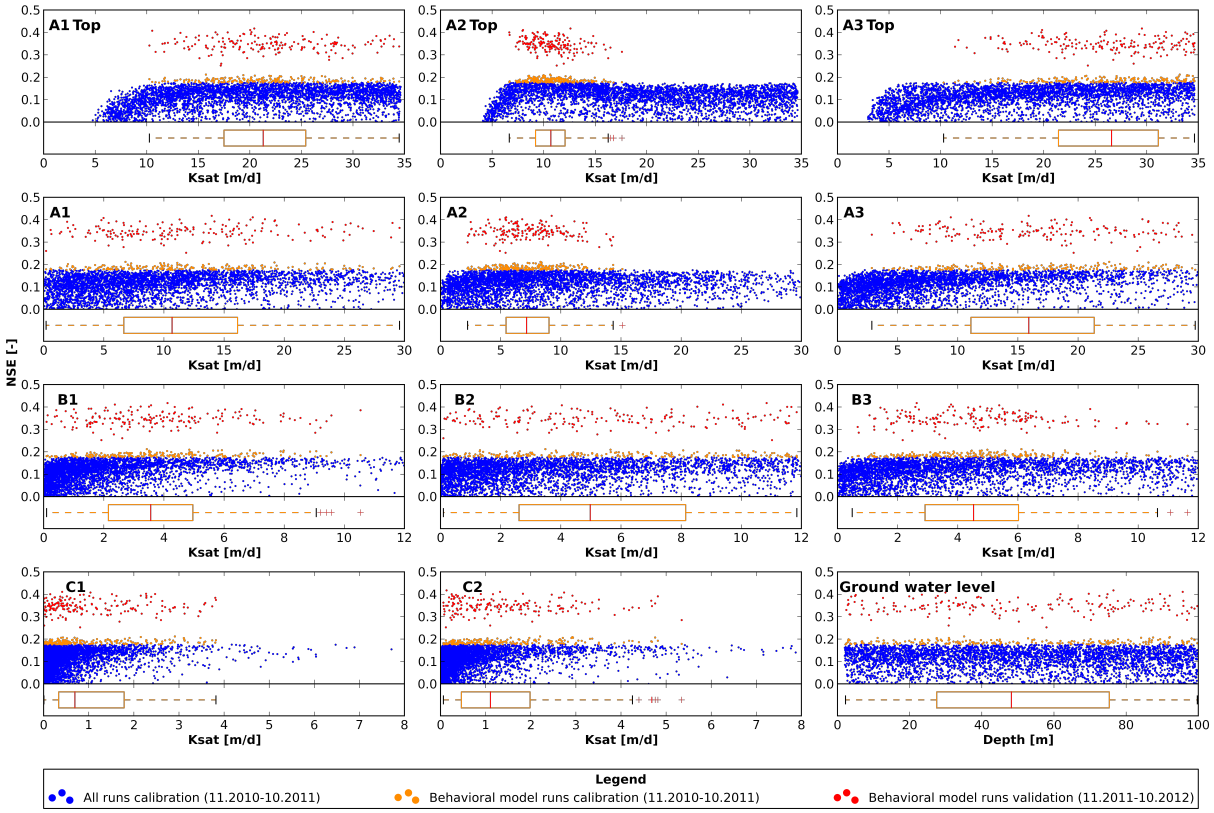

Figure 4 Dotty plots of NSE values (>0.0) during calibration (blue) and for behavioral model runs (NSE >0.15, bias <±20.0 ‰ δ^2H and R^2 > 0.65) during calibration (orange) and validation (red) for saturated hydraulic conductivity (K_{sat}) for all soil types and groundwater depth. Box plots show the unweighted parameter distribution of all behavioral model runs (NSE> 0.15, bias< ± 20.0 ‰ δ^2H and R^2 > 0.65). Results for soil porosity look similar to those of the groundwater and are therefore not shown.

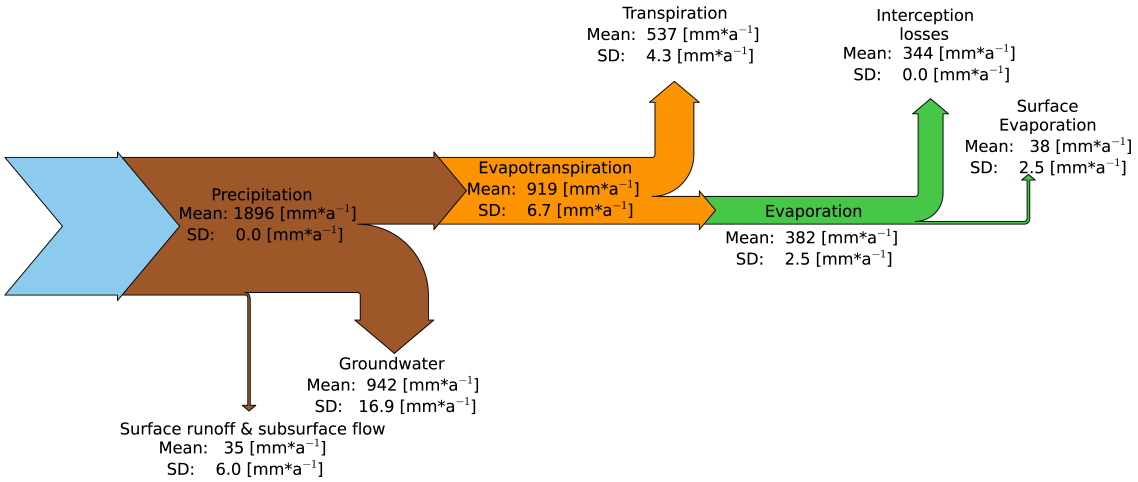

Figure 5 Mean annual flows and standard derivation (SD) of the main flow components at a hillslope scale of all behavioral model runs from 2010-2012.

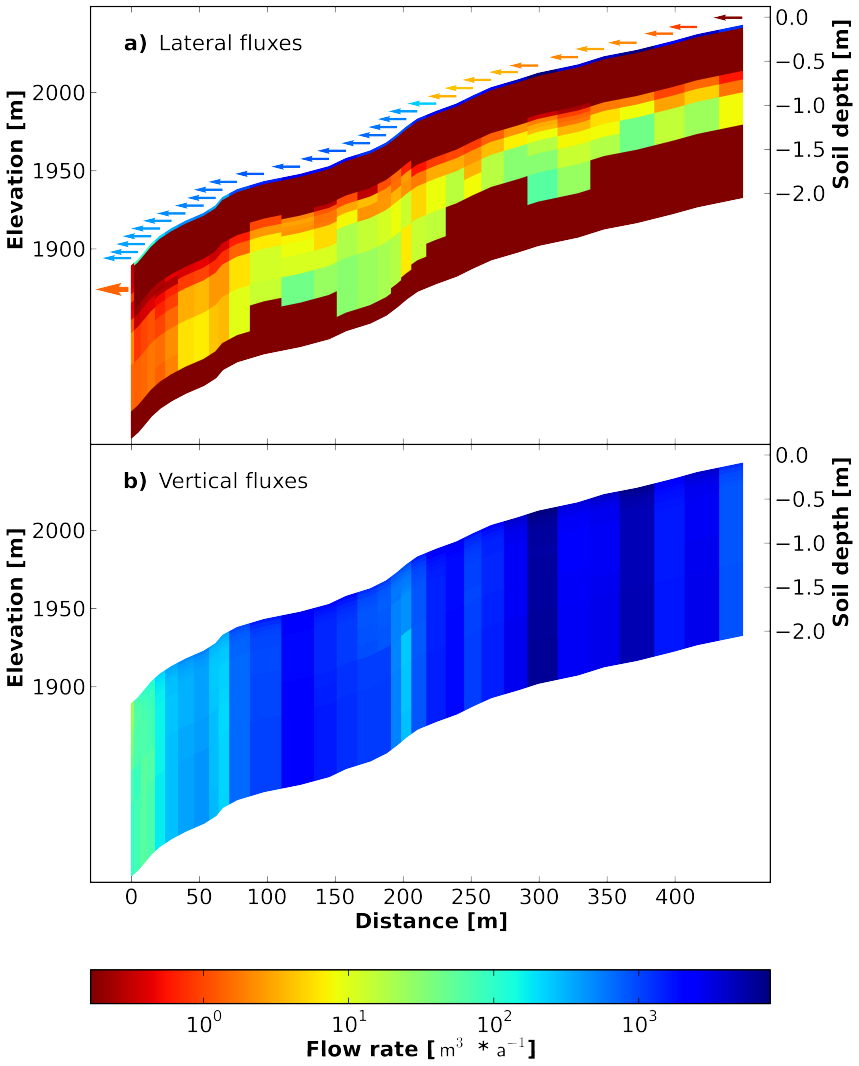

847

848 **Figure 6 a) Lateral and b) vertical fluxes for the best modeled fit. Arrows indicate the amount of surface runoff and**
849 **direct contribution to the outlet through subsurface flow. The maximum flow between storage compartments**
850 **is 7.3 10^3 m^3 a^{-1} and the total observed flow leaving as well as entering the system accumulates to 37 10^3 m^3 a^{-1}.**
851

852